Magnetic Field Analysis of PM Synchronous Motor with Eccentric PM Pole Shape Using Schwarz-Christoffel Transformation

Abdelouahab Tikellaline, Kamel Boughrara, Noureddine Takorabet, Baptiste Ristagno

Magnetic Field Analysis of PM Synchronous Motor with Eccentric PM Pole Shape Using Schwarz-Christoffel Transformation

Abdelouahab Tikellaline [1], Kamel Boughrara [2], Noureddine Takorabet [3] and Baptiste Ristagno [3]

[1] Université de Djilali Bounaama Khemis-Miliana (LESI), Route de Theniet El-had, Khemis-Miliana, 44225, Algeria
[2] Ecole Nationale Polytechnique (LRE-ENP), Algiers, 10, av. Pasteur, El Harrach, BP182, 16200, Algeria
[3] Université de Lorraine (GREEN), Vandoeuvre lès Nancy, France

This paper presents a magnetic field analysis of surface-mounted permanent magnet (PM) motor using Schwarz–Christoffel (SC) mapping method, taking account any eccentric PM shape and for varied magnetization pattern. Two rotor shapes with radial and parallel magnetization are proposed: The first has a conventional PM shape, while the other has an eccentric PM shape. For that, the calculated magnetic field in the middle of the air-gap using conformal mapping (CM) method and its harmonic content are compared for the four motors. Further, the influence of rotor shape and PM's magnetization on the back EMF and its harmonic content and on the cogging torque and electromagnetic torque is also discussed. Finally, finite-element method (FEM) is used to verify the obtained results, showing good agreement between both methods.

***Index Terms*— Permanent magnet (PM), eccentric PM shape, conformal mapping (CM), radial magnetization, parallel magnetization, equivalent current, cogging torque.**

I. Introduction

SURFAECE-MOUNTED permanent Magnet synchronous machine has been widely employed in industrial applications such as: aviation, wind turbines, and hybrid electric vehicle applications due to its high efficiency, high power factor and torque density. For designing PM motors and evaluating their efficiency, losses and vibrations, different methods have been developed for computing accurately the designed motor characteristics, such as magnetic field components, cogging torque and back-EMF. The modeling techniques can be classified as: 1) Numerical methods; 2) Semi-analytical models, and 3) Analytical methods.

Numerical methods (i.e., the finite-element (FE) [1], finite-difference [2]) are now widely applied in electrical machines design and they are very efficient because they take into account the complexity of geometry and the nonlinearity of the iron material, which lead to long CPU time. Therefore, numerical methods are not suitable for the first design stage and for use in optimization processes of the machine.

Although, in the first design stage, designers need a fast and accurate tools such as analytical methods (i.e., subdomain models [3] and Schwartz-Christoffel (SC) mapping [4]) which are suitable due to their accuracy and short calculation time.

Semi-analytical models (i.e., magnetic equivalent circuit (MEC) [5]) take into account magnetic saturation and calculate well enough the magnetic flux in different parts of the machine including iron parts. However, those methods cannot predict accurately the magnetic field in the air-gap and consequently it influences the accuracy of the predicted characteristics. For getting accurate results, semi-analytical models are combined with analytical models to compute accurately the magnetic field in the air-gap zone, such as subdomain models [6] or SC mapping [7].

Schwarz–Christoffel mapping is a complex mathematical function used to transform a complicated geometry into a simpler one to decrease complexity and solve problem easily.

Many authors used CM method for analyzing PM electrical machines [8-11]. The PMs, as an essential magnetic field source, affects the performances of the motor, such as magnetic field, back EMF and cogging torque, which results undesirable shaft vibration and acoustic noise. As a result, the choice of PM shape and magnetization pattern type is very important in PM motor design. The subdomain model used for considering radial and parallel magnetization patterns and slotting effect in a surface mounted PM machines is proposed and improved in [3]. Studies in [10] used an analytical SC mapping, which based on complex permeance of air-gap to analyze surface-mounted PM motor with radial magnetization, which shows a better much with FEM results and take into account the slotting effect, but it is limited to one slot and takes a long CPU time. Authors in [8, 9, 12] used the numerical SC mapping and the SC Matlab toolbox to analyze different surface-mounted PM rotating machines where the PMs have a radial magnetization and conventional shape, which give excellent results compared to FE Analysis.

However, few papers analyze the PM shapes and magnetization patterns influence in electrical motors. Chen *et al.* [13, 14] analyzed a surface-mounted PM synchronous machine with radial and parallel magnetized eccentric magnetic pole using the subdomain model with the scalar potential. Chikouche *et al.* [15] and Zhou *et al.* [16] used subdomain model with the vector potential to analyze different eccentric PMs with radial magnetization. However, Chikouche *et al* modeled the PM as sum of composed layers, while Zhou et al modeled the PM as equivalent currents.

Lizhan *et al* in [11] used SC toolbox to predict the thrust force of PM linear motor taking accounts for slotting effect, end effect and the magnet shape.

In past investigations, CM models have been developed for predicting the magnetic fields in PM machines without considering the magnet shape, and with including only radial magnetization pattern. In this paper, a SC mapping model is developed to predict the air-gap flux density in four surface-

TABLE I
MAIN DIMENSIONS AND PARAMETERS OF THE STUDIED MOTORS

Symbol	Value	Description
R_{se}	105 mm	Stator outer radius
R_s	75 mm	Stator inner radius
p	2	Number of pole pairs
Q_s	24	Number of slots
L	180 mm	Effective length of machine
h_{ys}	10 mm	Stator yoke height
h_{tt}	31.5 mm	Slot height
h_{tt}	2 mm	Tooth tip height
θ_s	7.8°	Slot opening
θ_{so}	5.45°	Semi-slot opening
R_r	66 mm	Rotor radius
α_{PM}	0.9	Pole-arc to pole-pitch ratio
h_{max}	6 mm	Magnet thickness (Max)
h_{min}	2 mm	Magnet thickness (Min)
B_r	1.2 T	Remanence of permanent magnet
M	Radial / Parallel	Magnetization
g	1.5 mm	Length of air gap

mounted PM motors with slotted stator and with concentric and eccentric shaped PM rotor. In the proposed model, PM excitation is replaced with equivalent current density according to Ampere's model. Although, any PM shape or magnetization pattern could be studied with the developed model. Therefore, the influence on air-gap flux density, cogging torque, electromagnetic torque and back-EMF waveform are investigated using SC mapping method.

II. CONFORMAL MAPPING TRANSFORMATIONS

The SC mapping is a mathematical transformation, which allows throw a series of transformation, the mapping of a complex air-gap structure of an electrical motor onto a simple geometry which analytic solutions are available. The electro-magnetic field is calculated in the canonical domain (ψ plane) and then it is mapped back to the original domain (S plane).

In this paper, the following assumptions are considered: Infinite permeable iron materials; Slot sides are radial; Linear properties of the PM; Relative permeability in the PM is equal to 1; Iron core saturation is neglected; Negligible end effect.

A. Logarithmic CM Transformation

The curved motor geometry in the S plane is mapped into multilateral geometry in the $W(u, v)$ plane using the following logarithmic CM function:

$$\omega = \log(s) \tag{1}$$

B. Numerical SC Transformation

The second step is the mapping of the canonical rectangle in the $Z(x, y)$ plane using the SC mapping function to the interior of polygon in the W plane using the SC mapping function [8]:

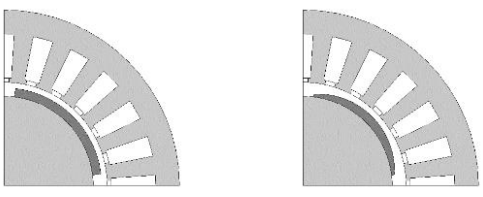

(a) (b)

Fig. 1. Cross section of proposed topologies. (a) Topology 1. (b) Topology 2

$$\omega = f(z) = A + C \int \prod_{k=1}^{n-1} (z - z_k)^{\alpha_k - 1}\, dz \tag{2}$$

C. Exponential CM Transformation

This transformation is used to map the interior of annular domain in ψ plane to rectangular domain in Z plane:

$$\psi = g^{-1}(z) = \exp\left(\frac{2\pi}{j\Delta x}\left(z - \frac{j\Delta y}{2}\right) - \frac{\pi}{j}\right) \tag{3}$$

III. PM SHAPES AND MAGNETIZATIONS UNDER INVESTIGATION

In this section, two surface-mounted PM motors, having the same stators configurations: 24-slot/ 4-pole combination, are considered. Fig. 1 shows the model of the studied motors, with two rotor configurations and two types of magnetizations for each rotor. The parameters of the motors are shown in Table I.

A. PM Shapes Geometry

The conventional magnet shape called Topo 1; O is the center of rotor and h_m is the radial magnet thickness, which does not change with position. For the eccentric magnet shape as shown in Fig. 1(b) called Topo 2 with radial sides, the magnet thickness changes with circumferential angle and the arc BC has a center O' placed on a distance H_x on the pole centerline from the center O, which makes the mathematical illustration becoming more difficult. For that, the geometrical relationships are performed according to [16].

IV. EXCITATION SOURCE MODELING

A. PM Excitation Modeling

The magnetic field produced by a PM having a magnetization M , is the same as that produced by a surface current density J_s [9] ($\vec{n}$ is the unit normal vector of the PM surface):

$$\vec{J_s} = \vec{M} \times \vec{n} \tag{4}$$

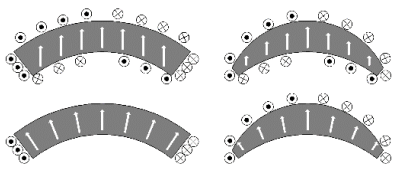

Fig. 2. Shapes and equivalent surface currents for PM Topologies 1, 2 with radial and parallel magnetization

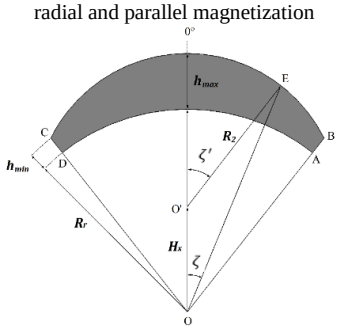

Fig. 3. Geometry of eccentric PM

According to (4), the equivalent surface currents of conventional PM pole shape (Topo 1) with radial and parallel magnetization and for eccentric magnet pole shape with radial and parallel magnetization (Topo 2) are shown in Fig. 2.

The equivalent surface-current method is based on a magnetic field produced by an equivalent coil [16]. Therefore, the current of each wire of the equivalent coil of a finite wires number n wire can be given by:

$$I_x = J_x.\Delta l \tag{5}$$

where Δl is the infinitesimal length between two adjacent surface currents. Table II gives J_x and Δl for all PMs.

V. Magnetic Field Solution

Hague has presented a magnetic field solution in a smooth air gap of a concentric cylinder machine [17] using three CMs including logarithmic, SC and an exponential transformations, to get a concentric cylindrical air-gap in the ψ plane. The scalar magnetic potential solution for arbitrary positioned current I_m in the air gap (annulus) defined in polar coordinates r and θ is given as [17]:

$$\Omega_\psi = \sum_{m=1}^{n} \frac{I_m}{2\pi}\left[\beta + \sum_{k=1}^{\infty}(A_k r^k + B_k r^{-k}).\sin(k.\Delta\theta)\right] \tag{6}$$

The flux density in the ψ plane is calculated from the scalar potential, and then mapped back to the original plane (S plane).

VI. Results and FE Validation

In order to validate the proposed method, the results obtained using the SC mapping are compared to those issued from 2D FEM. Figs. 4 and 5 show CM and FE predicted variation of the radial and tangential components of the flux density distribution in the middle of the air gap with both radial and parallel magnetizations during open-circuit condition. A very good agreement can be seen between the FE and the CM results

TABLE II
Punctual currents J_x and length Δl

Topology		Topology 1		Topology 2	
	Side	Radial	Parallel	Radial	Parallel
J_x	AB	$-M$	$-M.\cos\left(\frac{\theta_{PM}}{2}\right)$	$-M$	$-M$
	CD	M	$M.\cos\left(\frac{\theta_{PM}}{2}\right)$	M	M
	BC	0	$M.\sin(\zeta)$	$M.\sin(\zeta'-\zeta)$	$M.\sin(\zeta)$
	DA	0	$-M.\sin(\zeta)$	0	$M.\sin(\zeta')$
Δl	AB	$\frac{h_m}{n}$		$\frac{h_{min}}{n}$	
	CD	$\frac{h_m}{n}$		$\frac{h_{min}}{n}$	
	BC	$\frac{R_m.\theta_{PM}}{n}$		$\frac{R_2.2\zeta'_{PM}}{n}$	
	DA	$\frac{R_r.\theta_{PM}}{n}$		$\frac{R_r.\theta_{PM}}{n}$	

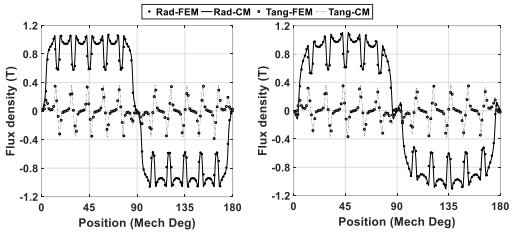

Fig. 4. Radial and tangential flux density distribution in the middle of the air-gap of topology 1 (left: radial magnetization, right: parallel magnetization)

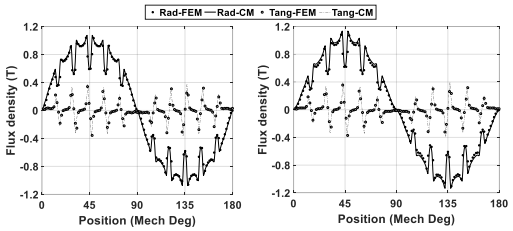

Fig. 5. Radial and tangential flux density distribution in the middle of the air-gap of topology 2 (left: radial magnetization, right: parallel magnetization)

The induced back EMF for no-load condition is calculated for every topology, Fig. 6 shows the comparison between analytically CM and FE predicted back-EMF at 1500 rpm. A good match between the CM results and the FE model can be observed. The total harmonic distortion (THD) of radial component of flux density is given in table III for the four motors. We can see that the motor of topology 2 has the lowest THD compared to the topology 1, a slight difference between THD of radial and parallel magnetization of topology 2. According to the table III, it can be found that topology 2 with parallel magnetization pattern could achieve more sinusoidal back-EMFs than the other topology with 5.32 % of THD.

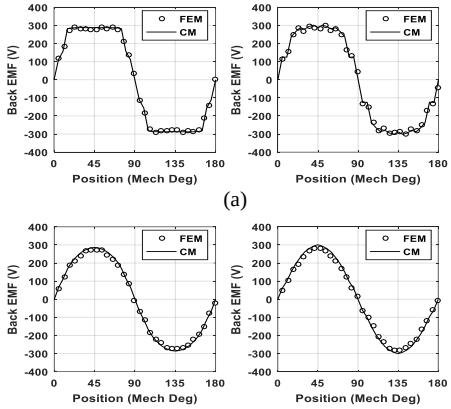

Fig. 6. Induced back EMF for no-load condition (left: radial magnetization, right: parallel magnetization): (a). Topology 1 (b). Topology 2

Fig. 7 shows the obtained electromagnetic torque produced by a sinusoidal armature current, it is clear that the motors with radial magnetization have more torque ripple compared to the motor with parallel magnetization. However, the torque waveforms of the SC mapping are slightly higher than the FE calculation due to the calculation of the back-EMF using winding theory at radius R_g which cause a small error by CM transformations.

TABLE III
RADIAL FLUX DENSITY AND BACK EMF THD COMPARISON

Topology	Topology 1		Topology 2	
Magnetization	Radial	Parallel	Radial	Parallel
Flux density THD (%)	39.94	31.12	20.11	18.33
Back EMF THD (%)	21.03	16.43	6.23	5.32

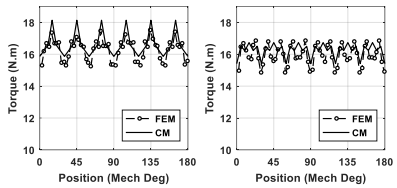

(a)

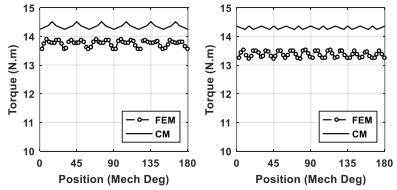

(b)

Fig. 7. Produced torque for max current of 5 A (left: radial magnetization, right: parallel magnetization): (a). Topology 1 (b). Topology 2

The obtained results using CM show that the electromagnetic torque decrease with eccentricity of magnet pole shape, Nevertheless, it can be found that topology 2 with parallel magnetization pattern has the minimum torque ripple with an average torque of 14.1 N.m. The obtained cogging torque of the four motors using CM and FE is shown in Fig. 8, a good agreement can be seen between both methods. It is found that PM shape affect significantly cogging torque. Also, topology with eccentric parallel PM has the lowest cogging torque peak and ripple.

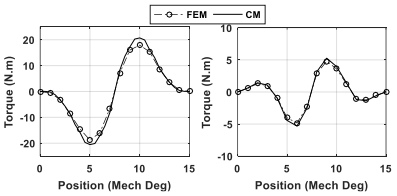

(a)

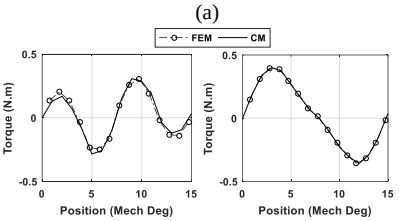

(b)

Fig. 8. Cogging torque (left: radial magnetization, right: parallel magnetization): (a). Topology 1 (b). Topology 2

VII. CONCLUSION

This paper has presented four topologies of surface mounted PM machines with different PM poles shapes and different magnetization patterns. An analytical method based on CM method has been proposed to predict the air-gap field distribution in those machines, taking into account concentric and eccentric geometry of PM, radial and parallel magnetization by replacing PM with equivalent surface currents. The investigation shows that the back EMF, cogging torque and electromagnetic torque are affected directly by PM shape and magnetization. The machine with eccentric PM and parallel magnetization has the lowest THD of radial flux density and back EMF and the lowest torque ripple. The obtained results are very satisfactory compared to FE results; the proposed method is appropriate in the preliminary design stage and can be used in optimization design procedure due to its short time calculation.

REFERENCES

[1] J. P. A. Bastos and N. Sadowski, *Electromagnetic modeling by finite element methods*: CRC press, 2003.

[2] M. N. Sadiku, *Numerical techniques in electromagnetics with MATLAB*: CRC press, 2011.

[3] T. L. Tiang, D. Ishak, C. P. Lim, and M. K. M. Jamil, "A comprehensive analytical subdomain model and its field solutions for surface-mounted permanent magnet machines," *IEEE Transactions on Magnetics*, vol. 51, pp. 1-14, 2015.

[4] M. Olivo, A. Tessarolo, and M. Bortolozzi, "On the use of conformai mapping in the analysis of electric machines," in *Electrical Machines (ICEM), 2016 XXII International Conference on*, 2016, pp. 492-498.

[5] V. Ostovic, *Dynamics of saturated electric machines*: Springer Science & Business Media, 2012.

[6] A. A. Diriye, S. Ouagued, Y. Amara, and G. Barakat, "Performance analysis of a series hybrid excited synchronous machine by a hybrid analytical model," in *2015 Tenth International Conference on Ecological Vehicles and Renewable Energies (EVER)*, 2015, pp. 1-6.

[7] A. Hanic, D. Zarko, and Z. Hanic, "A novel method for no-load magnetic field analysis of saturated surface permanent-magnet machines using conformal mapping and magnetic equivalent circuits," *IEEE Transactions on Energy Conversion*, vol. 31, pp. 740-749, 2016.

[8] K. Boughrara, D. Zarko, R. Ibtiouen, O. Touhami, and A. Rezzoug, "Magnetic field analysis of inset and surface-mounted permanent-magnet synchronous motors using Schwarz–Christoffel transformation," *IEEE Transactions on Magnetics*, vol. 45, pp. 3166-3178, 2009.

[9] M. Markovic, M. Jufer, and Y. Perriard, "Reducing the cogging torque in brushless DC motors by using conformal mappings," *IEEE Transactions on Magnetics*, vol. 40, pp. 451-455, 2004.

[10] D. Zarko, D. Ban, and T. A. Lipo, "Analytical calculation of magnetic field distribution in the slotted air gap of a surface permanent-magnet motor using complex relative air-gap permeance," *IEEE Transactions on Magnetics*, vol. 42, pp. 1828-1837, 2006.

[11] L. Zeng, X. Chen, X. Li, W. Jiang, and X. Luo, "A Thrust Force Analysis Method for Permanent Magnet Linear Motor Using Schwarz–Christoffel Mapping and Considering Slotting Effect, End Effect, and Magnet Shape," *IEEE Transactions on Magnetics*, vol. 51, pp. 1-9, 2015.

[12] K. Abbaszadeh and F. R. Alam, "On-load field component separation in surface-mounted permanent-magnet motors using an improved conformal mapping method," *IEEE Transactions on Magnetics*, vol. 52, pp. 1-12, 2016.

[13] Z. Chen, C. Xia, Q. Geng, and Y. Yan, "Modeling and analyzing of surface-mounted permanent-magnet synchronous machines with optimized magnetic pole shape," *IEEE Transactions on Magnetics*, vol. 50, pp. 1-4, 2014.

[14] Z. Chen, Z. Li, H. Ma, and Y. Guo, "Optimization and analysis of permanent-magnet synchronous machine with eccentric magnetic pole shape," in *Electrical Machines and Systems (ICEMS), 2015 18th International Conference on*, 2015, pp. 1181-1186.

[15] B. L. Chikouche, K. Boughrara, and R. Ibtiouen, "Cogging torque minimization of surface-mounted permanent magnet synchronous machines using hybrid magnet shapes," *Progress In Electromagnetics Research B*, vol. 62, pp. 49-61, 2015.

[16] Y. Zhou, H. Li, G. Meng, S. Zhou, and Q. Cao, "Analytical calculation of magnetic field and cogging torque in surface-mounted permanent-magnet machines accounting for any eccentric rotor shape," *IEEE Transactions on Industrial Electronics*, vol. 62, pp. 3438-3447, 2015.

[17] B. Hague, "The principles of electromagnetism applied to electrical machines," 1962.